Observation of Reduced Core Electron Temperature Fluctuations and Intermediate Wavenumber Density Fluctuations in H- and QH-mode Plasmas

L. Schmitz 1), A.E. White 1), G. Wang 1), J.C. DeBoo 2), G.R. McKee 3), J.S. deGrassie 2), J.C. Hillesheim 1), W.A. Peebles 1), T.L. Rhodes 1), C.C. Petty 1), L. Zeng 1), E.J. Doyle 1), T.A. Carter 1), K.H. Burrell 2), W.M. Solomon 4), J.E. Kinsey 2), G.M. Staebler 2), and the DIII-D Team

1) University of California, Los Angeles, Los Angeles, California 90095-1547, USA
2) General Atomics, San Diego, California 92186-5608, USA
3) University of Wisconsin-Madison, Madison, Wisconsin 53706, USA
4) Princeton Plasma Physics Laboratory, Princeton, New Jersey 08543-0451, USA

e-mail contact of main author: lschmitz@ucla.edu

Abstract. In this paper, we report observations of reduced low-k core electron temperature and intermediate-k density fluctuations in H-mode and quiescent (QH)-mode. L-mode electron temperature fluctuation levels ($0.5\% \leq \tilde{T}_e/T_e \leq 2\%$ for $k_\theta \rho_s \leq 0.5$ as measured by correlation ECE (CECE) radiometry) are observed to decrease by at least a factor of four in H and QH-mode regimes in the DIII-D tokamak ($r/a = 0.7$). Recent results from DIII-D provide the first experimental evidence that, in addition, intermediate-scale turbulence ($0.5 < k_\theta \rho_s \leq 3$) is also reduced promptly at the L-H transition. A 20%–30% prompt reduction ($r/a > 0.7$) has been found at the L-H transition in co-injected plasmas, with a larger decrease (~75%) observed near the pedestal top. Very substantial reductions have been observed in the core of counter-injected, low-density QH-mode plasmas ($r/a < 0.8$) at the L-H transition, and suppression has been observed for $r/a \leq 0.5$. Experimental results and linear stability calculations (using the TGLF trapped gyro-Landau fluid code) indicate that intermediate/small scale turbulence persists in H-mode at a reduced amplitude for $r/a > 0.5$ and may dominate residual anomalous electron heat transport in the QH-mode plasmas examined here.

1. Introduction

Electron heat transport in tokamaks is anomalous and thought to result from plasma turbulence. Large-scale fluctuations in tokamaks [$k_\theta \rho_s \leq 0.3$, where $\rho_s = c_s m_i / eB_T$ with $c_s = (kT_e/m_i)^{1/2}$] are known to be locally reduced as the edge transport barrier forms during the L- to H-mode transition [1,2]. This reduction occurs as plasma rotation and rotational $\boldsymbol{E}\times\boldsymbol{B}$ shear increase in the pedestal region and, in quiescent H-mode (QH-mode), further into the core plasma [3]. It has been invoked as an explanation of the reduced particle and ion heat transport observed in H- and QH-mode. Previous studies of turbulence behavior across the L- to H-mode transition have mainly focused on large-scale density fluctuations associated with ion temperature gradient (ITG) driven turbulence which is thought to dominate anomalous L-mode transport [4]. Recently, multi-scale gyrokinetic simulations [5–7] have suggested that both large scale and intermediate/small-scale fluctuations can contribute to anomalous electron heat transport. Shear stabilization is ineffective or less effective for small scale turbulence due to the high linear growth rates (compared to the achievable $\boldsymbol{E}\times\boldsymbol{B}$ shearing rates) and small size of the turbulent eddies. The contribution of intermediate/small scale fluctuations [trapped electron modes (TEM) and electron temperature gradient (ETG) modes] is thought to dominate electron heat transport in plasmas with core transport barriers [8] and/or strong central electron heating [9,10]. It is also expected to be important in other plasma regimes once large-scale turbulence has been reduced or suppressed by rotational $\boldsymbol{E}\times\boldsymbol{B}$ shear [5,6] and may be important in burning plasmas where α-particle heating primarily

affects the electron channel. In this paper we report two new observations relevant to anomalous electron heat transport. We have observed substantially reduced low wavenumber ($k_\theta \rho_s \leq 0.5$) core electron temperature fluctuations across the L- to H-mode transition [11] simultaneously with reduced electron heat diffusivity. These measurements have been obtained using correlation electron cyclotron emission (CECE) radiometry. Our observations suggest that electron temperature fluctuations can contribute substantially to L-mode electron heat transport. In addition, we have observed a significant reduction in intermediate-scale core density fluctuations in H- and QH-mode plasmas. We present recent Doppler backscattering (DBS) data indicating that intermediate scale density fluctuations ($1 \leq k_\theta \rho_s \leq 3$) are reduced substantially in H- and quiescent H-mode (QH-mode) compared to L-mode, but persist at a lower level. This reduction is most pronounced at the top of the pedestal but a significant reduction in the core plasma fluctuation level has been observed for $(0.4–0.8) \leq r/a \leq 1$, depending on the specific plasma conditions. Intermediate scale fluctuation suppression has been observed for $r/a < 0.5$ in counter-injected, low density QH-mode plasmas ($k_\theta \rho_s \sim 2$). Results of linear stability calculations with the trapped gyro-Landau fluid code TGLF [12,13] for the low and intermediate/high wavenumber range are presented.

2. Electron Temperature Fluctuation Measurements

Experiments and gyrokinetic simulations are beginning to establish the role of core electron temperature fluctuations for anomalous electron heat transport [11,14,15]. The anomalous electron heat flux can be expressed as [16]

$$Q_e^{fl} = 3/2\left(nk_B T_e\right)/B_T \left[\left\langle \left(\tilde{T}_e/T\right)\tilde{E}_\theta \right\rangle + \left\langle \left(\tilde{n}/n\right)\tilde{E}_\theta \right\rangle\right] \quad . \tag{1}$$

Here, n, T_e and B_T are the density, electron temperature, and toroidal magnetic field, respectively, and $\tilde{n}$, $\tilde{T}_e$, and $\tilde{E}_\theta$ are the density, electron temperature, and poloidal electric field fluctuation levels, with the brackets denoting a time average. The relative contribution of density and temperature fluctuations to thermal transport depends on the cross-phase between temperature/density fluctuations and poloidal electric field fluctuations but $\tilde{T}_e$ and $\tilde{n}_e$ fluctuations can potentially contribute equally to the observed anomalous electron heat transport.

The local electron temperature in tokamaks is routinely measured with high time resolution using electron cyclotron emission (ECE). However, the detection of broadband electron temperature fluctuations in tokamaks requires the extraction of spatially correlated fluctuations from the thermal fluctuations inherent in cyclotron emission. A correlation technique (correlation electron cyclotron emission (CECE) [17,18]) is therefore required. CECE measurements have been performed in upper single null, beam-heated discharges in the L-mode H-mode, and QH-mode regimes (Fig. 1). The QH-mode regime is characterized by the absence of edge-localized modes (ELMs), which, in a regular H-mode, typically begin within a few hundred ms after the L- to H-mode transition. In this discharge, the L- to H-mode transition is preceded by a 500 ms long L-mode phase. Neutral beam power (2.6 MW) is counter-injected (oriented opposite the plasma current) at 400 ms followed by the addition of a second 2.1 MW counter-beam source at 800 ms. The H-mode transition occurs at t = 900 ms as indicated by the sudden drop in the midplane deuterium D_α emission intensity [Fig. 1(d)]. During H-mode, the line-averaged density increases threefold due to improved particle confinement. The central electron and ion temperatures increase from 1.5 keV to 3.8 keV, and

from 1.5 keV to 12 keV, respectively, and the global energy confinement time increases by a factor of 2.5–3.0 after the H-mode transition and during the QH-mode phase, compared to the L-mode value.

The relative temperature fluctuation amplitude is given by the correlation coefficient of the CECE signals $C_{12}(\Delta t)$ [17,19] at zero time delay (Δt = 0), according to $\tilde{T}_R/T_R = [C_{12}(\Delta t{=}0)]^{1/2} \times (B_v/B_{IF})^{1/2}$, where B_v is the video bandwidth and B_{IF} is the intermediate frequency bandwidth [11,17].

The CECE diagnostic is most sensitive to low-k ITG/TEM turbulence ($k_\theta\rho_s \leq 0.25$ in L-mode and $k_\theta\rho_s \leq 0.5$ in H- and QH-mode). The measurements reported here show that during L-mode operation low-k relative temperature fluctuation levels are similar in magnitude to low-k density fluctuations levels, as discussed in detail elsewhere [15].

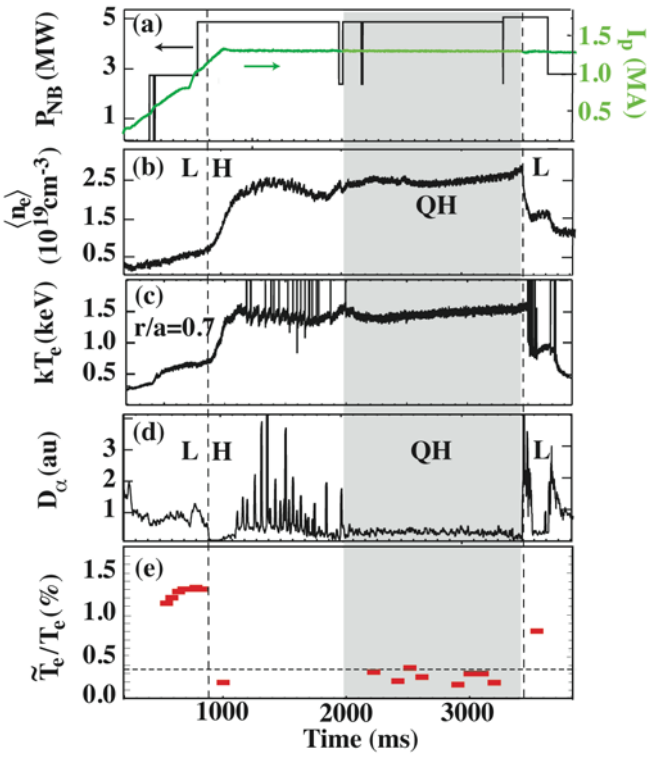

FIG. 1. (a) Neutral beam power and plasma current; (b) line-averaged density; (c) electron temperature at r/a=0.7; (d) D_α line emission intensity; (e) normalized electron temperature fluctuation level (r/a=0.7) for shot #125113. L-H and H-L transitions are indicated by vertical dashed lines, the QH-mode phase is shaded.

Linear stability calculations with the TGLF code [12,13] have been carried out for the L-mode and QH-mode phases, indicating that the observed low L-mode temperature fluctuations ($k_\theta\rho_s \leq 0.3$) can be attributed to ion temperature gradient (ITG) modes stabilized by rotational ***E×B*** shear at the L-H-mode transition. A comparison of the normalized linear growth rates with the flux-surface-averaged shearing rate $\omega_{ExB} = \left\langle [(RB_\theta)^2/B](\partial/\partial\psi)\,(E_r/RB_\theta)\right\rangle$, calculated using charge exchange recombination (CER) spectroscopy data, is shown in Fig. 2. Here, R is the major radius, B_θ is the poloidal magnetic field, E_r is the radial electric field, and a is the minor plasma radius. γ_e and γ_i denote the linear ITG and electron mode (TEM/ETG) growth rates. In L-mode, the ***E×B*** flow shear is insufficient to suppress ITG and TEM/ETG-modes (R/L_n = 1.5, R/L_{Te} = 6.3, where L_n and L_{Te} are the density and electron temperature gradient scale lengths, respectively), but ITG modes are expected to dominate transport due to the longer wavelength. In contrast, TGLF results indicate that TEM and/or ETG modes dominate linear stability in H and QH-mode ($R/L_n \sim 1$, R/L_{Te} = 4). Here, the shearing rate is found to exceed the calculated linear ITG growth rate by a large factor. Stabilization of electron modes is expected for $k_\theta\rho_s \leq 1.2$, but for higher values of $k_\theta\rho_s$ the linear growth rate exceeds the shearing rate. The observed reduction of $\tilde{T}_e$ at the transition to H-mode suggests that temperature fluctuations potentially play a major role in the improved confinement properties observed during H- and QH-mode operation [11]. Figure 3 shows a plot of the electron thermal diffusivity in L and QH-mode, obtained from transport analysis using the ONETWO code [21]. It is found that the electron heat diffusivity is substantially reduced from L-mode values during QH-mode ($\chi_e^{QH}/\chi_e^{L} < 0.25$). The ratio of the maximum linear growth rate in the wavenumber range accessible by CECE to the ***E×B***

shearing rate is also shown in Fig. 2. It is clear from Fig. 2(b) that smaller-scale modes ($k_\theta \rho_s \geq 1.2$) are still expected to be unstable in H/QH-mode and may contribute to the residual anomalous electron heat flux in these regimes.

3. Intermediate Scale Density Fluctuation Levels

The potential role of intermediate/small scale TEM/ETG modes for electron heat transport has been investigated experimentally for plasma regimes with central electron transport barriers [8], and for Electron Cyclotron Resonance (ECH)-heated plasmas [10,22]. Local measurements of intermediate/smaller scale density fluctuations have not been previously made in H-mode. We report measurements of intermediate scale density fluctuations ($0.5 \leq k_\theta \rho_s \leq 3.0$) using Doppler backscattering (DBS). A microwave beam launched at an oblique angle to the magnetic flux surfaces is backscattered at the O-mode (or X-mode) cut-off layer in the plasma. The backscattered signal is received via the same antenna and beam optics. Hence, the wavenumber k_r of the backscattered signal is related to the wavenumber of the incident signal k_i according to the selection rule k_r=-k_i. Due to refraction, the incident beam is deflected in the poloidal plane as it propagates in the plasma. Backscattering at the cut-off layer occurs only for the resonant poloidal fluctuation wavenumber k_θ=-2k_i. The GENRAY ray-tracing code [23] is used to determine the location of the cut-off layer as well as the local wavenumber k_r=-k_i at the reflection point. The frequency of the backscattered signal ω_r is determined by the Doppler-shifted resonant mode frequency according to $\omega_r = \omega_I + k_\theta(v_{ph}+v_{ExB})$, where v_{ph} and v_{ExB} are the mode perpendicular phase velocity and the ***E×B*** speed. In the core of beam-heated DIII-D plasmas v_{ExB} by far dominates the mode phase velocity which is neglected here.

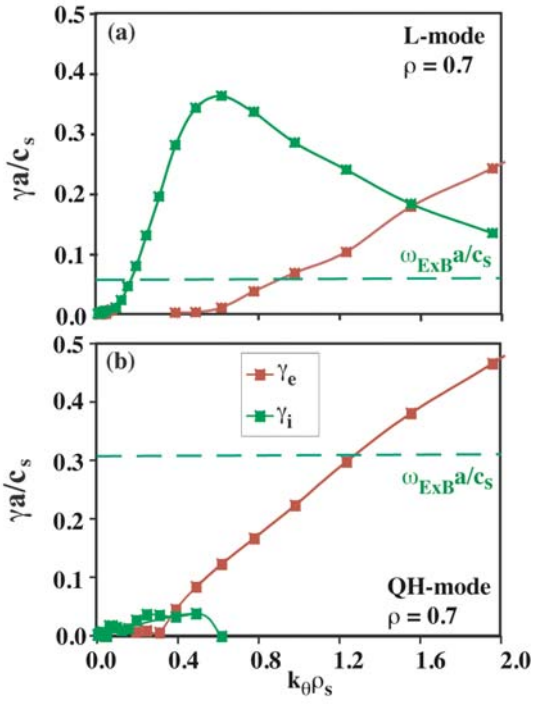

FIG. 2. Linear growth rates for ion (ITG) and electron modes calculated with the TGLF code for L-mode (725 ms) and QH-mode (2500 ms) and comparison with the ***E×B*** shearing rate.

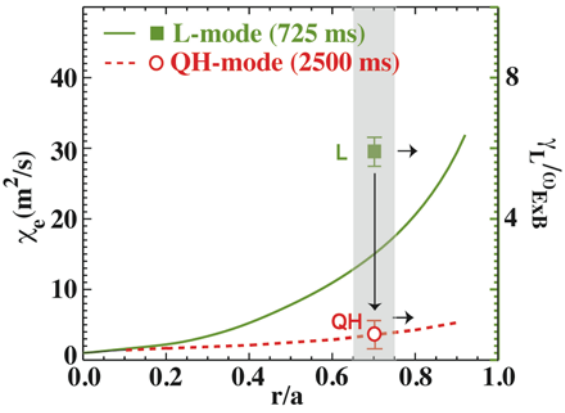

FIG. 3. Electron heat diffusivity and ratio of linear maximum linear growth rate γ_L to ***ExB*** shearing rate in L-mode (solid line) and QH-mode (dashed line).

Figure 4 shows the evolution of intermediate scale and large scale (low-k) density fluctuation levels across the L-H transition in a co-injected plasma (B_T = 2 T, I_p = 1 MA, P_{NB} = 3 MW), obtained with O-mode DBS. The 42 GHz back-scattered signal (proportional to the density fluctuation level at $k_\theta \sim 7$ cm^{-1}, $k_\theta \rho_s \sim 0.8$ with a resolution $\Delta k_\theta \leq 1.5$ cm^{-1}) localized at $r/a \sim 0.7$ decreases simultaneously with the reduction of the D_α signal on a 1 ms

timescale [Fig. 4(a)]. After the transition to H-mode as the density pedestal evolves, the measurement location (determined by the 42 GHz O-mode cut-off) moves radially outward due to increasing plasma density. The backscattered signal initially increases during this outward movement indicating increasing density fluctuation levels as the edge pedestal region is approached. However, a large reduction is seen as the probing location reaches the top of the pedestal (r/a = 0.9). A second intermediate-k signal [Fig. 4(b), $k_\theta \sim 3$ cm^{-1}, $k_\theta\rho_s \sim 0.4$–0.6, localized in the pedestal at $r/a \sim 0.95$ in L- and H-mode) shows an order-of-magnitude reduction at the transition on a 100 μs timescale. For comparison, the reduction of low wavenumber ($k_\theta\rho_s < 0.3$) density fluctuations in the pedestal, as measured by beam emission spectroscopy (BES) is shown in Fig. 4(c). The BES data also shows incidental long wavelength MHD modes ($t > 2150$ ms) not seen on the DBS signals sensitive to a narrow intermediate wave-number range. Backscattering data and FIR scattering data (not shown) indicate reductions of $\tilde{n}/n$ in the core plasma ($r/a \leq 0.65$) at higher poloidal wavenumber ($k_\theta > 7$ cm^{-1}, $k_\theta\rho_s \geq 1.5$) in this intermediate-k (TEM/ETG) range.

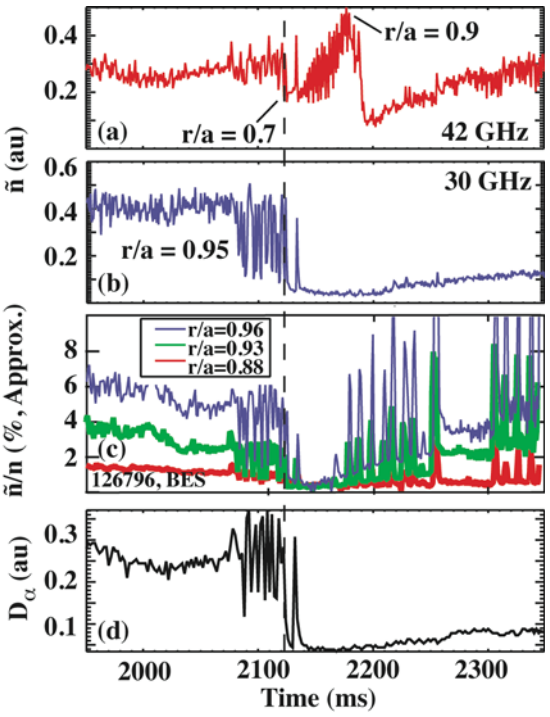

FIG. 4. (a) Backscattered signal (f = 42 GHz with cut-off present, localized as shown, $k_\theta \sim 6$ cm^{-1} (r/a~0.7, 2100 ms), $k_\theta \sim 4$ cm^{-1} (r/a~0.9, 2170 ms); (b) 30 GHz (r/a=0.95, $k_\theta \sim 3$ cm^{-1}); (c) relative density fluctuation level at low wave-number $k_\theta < 3$ cm^{-1} (BES); (d) D$_\alpha$ signal across the L-H transition (dashed line).

A radial profile of the intermediate-k density fluctuation level after the H-mode transition in arbitrary units, obtained from mapping the time evolution (2130–2200 ms) of the data shown in Fig. 1(a) using profile reflectometry, is shown in Fig. 5. This data demonstrates a moderate increase of fluctuation level with radius in H-mode for $r/a < 0.9$, and a substantial decrease with radius near the pedestal top. For comparison, the L-mode fluctuation level is $\tilde{n} = 0.33$ (au) (r/a = 0.7, 2100 ms), and 0.75 (au) (r/a = 0.95, 2100 ms).

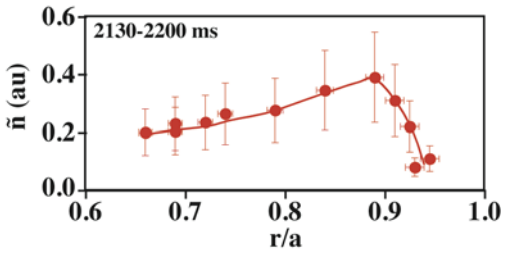

FIG. 5. Radial profile of intermediate-k density fluctuation level in H-mode; the error bars represent uncertainties in the scattering volume.

More recently we have observed very substantial reductions of intermediate scale density fluctuation levels in the core of counter-injected low-density QH-mode plasmas. Figures 6 and 7 show DBS spectra across the L-H transition ($0.35 \leq r/a \leq 0.8$, 4.5 cm^{-1} $\leq k_\theta \leq$ 7.5 cm^{-1}, $0.8 \leq k_\theta\rho_s < 2$) from two similar discharges. Figure 6 shows data obtained launching a constant probing frequency (f = 64.9 GHz, X-mode). The DBS feature is shifted to positive frequencies; a comparison with the over-plotted Charge Exchange Recombination Spectroscopy (CER) data indicates that the Doppler frequency shift f_D is consistent with the

E×B drift due to the negative core radial electric field in the plasma ($f_D \sim k_\theta v_{ExB}/2\pi$). The probing location is $r/a \sim 0.35$ (1000–1050 ms, probed $k_\theta\rho_s \sim 1.5$) before the H-mode transition, $r/a \sim 0.4$ at 1100 ms ($k_\theta\rho_s \sim 1.9$), $r/a \sim 0.45$ at 1175 ms ($k_\theta\rho_s \sim 1.7$), and $r/a \sim 0.53$ at 1200 ms ($k_\theta\rho_s \sim 1.5$). Intermediate-scale core fluctuations are initially observed as intermittent bursts for $r/a \leq 0.5$, although the plasma is free of sawtooth oscillations. Within ~10 ms of the L-H transition, the DBS spectrum indicates substantial reduction or elimination of fluctuations for $r/a \leq 0.45$. However, intermediate-scale turbulence persists at larger minor radii for slightly lower values of probed $k_\theta\rho_s$.

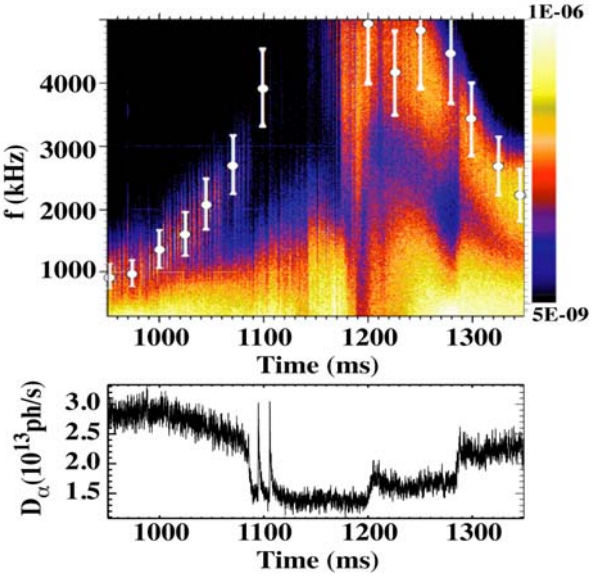

FIG. 6. Doppler spectrum vs time across the L-H transition in a low density QH-mode shot (#131902, $0.35 \leq r/a \leq 0.8$). f_{ExB} from CER is indicated by white symbols. Also shown is the D_α signal indicating the transition timing.

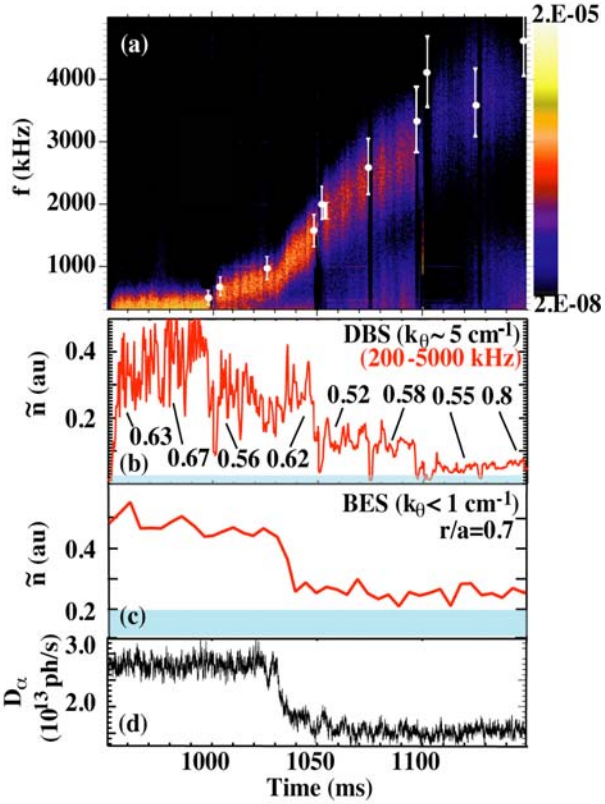

FIG. 7. (a) Doppler spectrum vs time (f_{ExB} from CER is indicated by white symbols), (b) intermediate scale fluctuation level ($0.52 \leq r/a \leq 0.8$ as indicated), (c) low-k (< 1 cm^{-1}) fluctuation level from BES, and (d) D_α signal across the L-H transition in a low density QH-mode shot (#131912). The sensitivity/noise level is indicated in (b) and (c).

Reduced turbulence is observed outside and within the region of negative central magnetic shear ($r/a \leq 0.45$ for $t = 1200$ ms). For the data shown in Fig. 7, the probing frequency was stepped to obtain data across the L-H transition for $0.5 \leq r/a \leq 0.8$. The DBS spectrum [Fig. 7(b)] again indicates fluctuation reduction within ~10 ms after the L-H transition. For comparison, the low-*k* fluctuation level from BES (k_θ < 1 cm^{-1} in this counter-injected plasma with reversed I_p), is shown. The BES signal shows prompt reduction which is consistent with the expectation that the increasing ***E×B*** shear affects low-*k* modes prior to intermediate-*k* modes. The extracted (relative) fluctuation levels are shown in Fig. 8. While the L-mode data are taken at lower values of $k_\theta\rho_s$ ($0.7 \leq k_\theta\rho_s \leq 0.95$) than the H-mode data ($0.8 \leq k_\theta\rho_s \leq 1.4$) due to the increased electron temperature in H-mode, this difference does not account for the observed change in fluctuation level even if a spectral dependence of the fluctuation level $(\tilde{n}/n)^2 \sim (k_\theta\rho_s)^{-3}$ is

assumed [24]. The frequency shift calculated from CER data $f_{ExB} = k_\theta v_{ExB}/2\pi$, as indicated by white symbols, again agrees well with the frequencies observed by DBS.

In the following, we present linear stability calculations and a comparison of the linear growth rate and the ***E×B*** shearing rate for L- and H-mode. Figures 9 and 10 show TGLF calculations for $r/a = 0.4$ and $r/a = 0.7$. The growth rate of the most unstable mode is shown in comparison to the flux-surface-averaged shearing rate. Unstable modes in the ITG and TEM/ETG regime are expected at small minor radius (r/a =0.4) in L-mode ($R/L_n = 2.6$, $R/L_{Te} = 4.3$) while stability is expected for $k_\theta\rho_s \leq 4$ in H/QH- mode ($R/L_n = 1.7$, $R/L_{Te} = 2$), in agreement with our experimental findings for intermediate-scale modes (Fig. 6). In contrast, at $r/a = 0.7$ the plasma is predicted to be unstable for $k_\theta\rho_s \geq 0.35$ in L-mode ($R/L_n = 2.1$, $R/L_{Te} = 4.9$) and for $k_\theta\rho_s \geq 1.1$ in QH-mode ($R/L_n = 1$, $R/L_{Te} = 4.4$), consistent with the experimental observation of intermediate-scale modes persisting in H/QH-mode. These calculations support the dominance of intermediate-scale fluctuations in H- and QH-mode and also the experimental observation of reduced fluctuation level compared to the L-mode phase for $0.5 \leq r/a \leq 0.8$. It should be noted that considerable ***E×B*** shear is already present in L-mode for the time slice chosen (875 ms), in advance of the L-H transition occurring at 1030 ms.

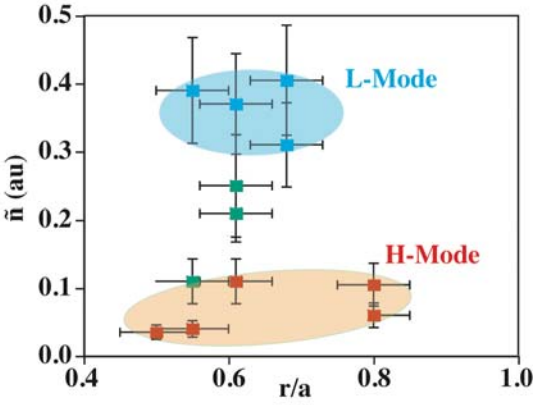

FIG. 8. Measured intermediate-scale fluctuation levels in L- and H-mode (#131912). Data from the L-H transition period are also included (green symbols).

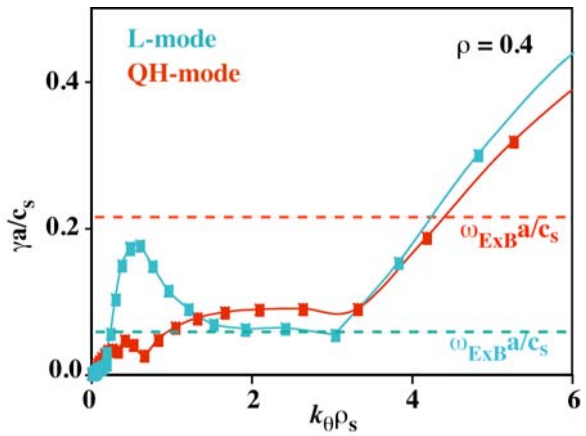

FIG. 9. Linear growth rate of the most unstable mode in L-mode (875 ms) and H-mode (1200 ms) calculated from TGLF for $r/a = 0.4$ in comparison to flux-surface-averaged ***E×B*** shearing rate.

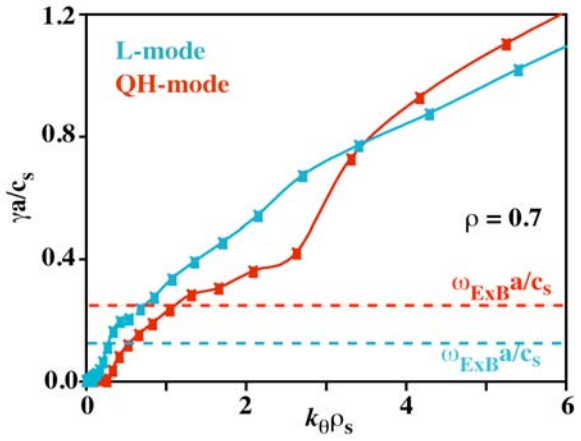

FIG. 10. Linear growth rate of the most unstable mode in L-mode (875 ms) and H-mode (1200 ms) calculated from TGLF for $r/a = 0.7$ in comparison to flux-surface-averaged ***E×B*** shearing rate.

4. Conclusions

We have presented experimental evidence of reduced low-k core electron temperature fluctuations and intermediate-scale density fluctuations in H- and QH-mode. The observation of electron temperature fluctuations in ITG-dominated L-mode plasmas may be indicative of a non-adiabatic electron response associated with trapping effects, and suggests that these fluctuations contribute substantially to L-mode electron heat transport. Intermediate-scale turbulence is found to be substantially reduced and eliminated for $r/a \leq 0.5$ in low-density, counter-injected H/QH-mode plasmas. TGLF calculations suggest that these fluctuations are related to electron-driven modes. The persistence of these modes in plasmas where low-k turbulence is stabilized by $\boldsymbol{E}\times\boldsymbol{B}$ flow shear suggests that intermediate-scale turbulence contributes to or dominates the residual core electron heat transport during H- and QH-mode in the plasmas investigated here. Local (flux-tube) gyrokinetic simulations are presently under way to separately predict the contributions of low-k and intermediate-k fluctuations to electron heat loss and to enable quantitative comparisons with experimentally observed electron transport fluxes and fluctuation levels.

Acknowledgments

This work was supported by the US Department of Energy under DE-FG03-01ER54615, DE-FG02-89ER53296, DE-FC02-04ER54698, DE-FG02-08ER54984, DE-AC02-76CH03073 and General Atomics subcontract NS53250.

References

[1] DOYLE, E.J., *et al.,* Phys. Fluids B **3**, 2307 (1991).
[2] RETTIG, C.L., *et al.*, Nucl. Fusion **33**, 643 (1993).
[3] BURRELL, K.H., *et al.*, Plasma Phys. Control. Fusion **46**, 165 (2004).
[4] CANDY, J. and WALTZ, R.E., Phys. Rev. Lett. **91**, 045001 (2003).
[5] GOERLER, T. and JENKO, F., Phys. Rev. Lett. **100**, 185002 (2008).
[6] WALTZ, R.E., *et al.*, Phys. Plasmas **14**, 056116 (2007).
[7] KINSEY, J.E., *et al.*, Phys. Plasmas **15**, 055908 (2008).
[8] ERNST, D.R., *et al.*, Phys. Plasmas **11**, 26377 (2004).
[9] PEETERS, A.G., *et al.*, Phys. Plasmas **12**, 022505 (2005).
[10] RYTER, F., *et al.*, Phys. Rev. Lett. **95**, 085001 (2005).
[11] SCHMITZ, L., *et al.*, Phys. Rev. Lett. **100**, 035002) (2008).
[12] STAEBLER, G.M., *et al.*, Phys. Plasmas **12**, 102508 (2005).
[13] STAEBLER, G.M., *et al.*, Phys. Plasmas **14**, 055909 (2007).
[14] WHITE. A.E., *et al.,* Phys. Plasmas **15**, 056116 (2008).
[15] HOLLAND, C., *et al.*, this conference.
[16] ROSS, D.W., Plasma Phys. Control. Fusion **34**, 137 (1992).
[17] SATTLER, S., *et al.,* Phys. Rev. Lett. **72**, 653 (1994).
[18] CIMA, G., et al., Phys. Plasmas **2**, 720 (1995).
[19] BEKEFI, G., *Radiation Processes in Plasmas* (Wiley, New York, 1966).
[20] BENDAT, J.S and PIERSOL, A.G., *Random Data: Analysis and Measurement Procedures* (Wiley, New York, 1986).
[21] ST JOHN, H.E., *et al.,* Plasma Phys. Control. Nucl. Fusion Research **3**, 603 (1994).
[22] RHODES, T.L., *et al.,* Phys. Plasmas **14**, 056117 (2007).
[23] SMIRNOV, A.P. and HARVEY, R.W., "The GENRAY Ray Tracing Code," CompX Report COMPX-2000-01 (2001).
[24] HENNEQUIN, P., *et al.,* Nucl. Fusion **46**, S771 (2006).